Direct measurement of disk-to-head back-heating in HAMR using a non-flying test stage

Qilong Cheng,[a] Siddhesh V. Sakhalkar, and David B. Bogy
University of California at Berkeley, Berkeley, California 94720, USA.

(Dated: 4 April 2022)

Heat assisted magnetic recording (HAMR), as one of the next generation hard disk drive solutions to high areal density over 1 Tb/in^2, integrates a laser delivery system to facilitate data writing. A laser beam is launched from the recording head and is focused on the recording disk to locally heat the disk (400–500 °C), which is even hotter than the head temperature (150–250 °C). Therefore, understanding the thermal transport between the head and the disk is of great importance. In this paper, we used a non-flying test stage to exclude the strong air cooling caused by the rotating disk, and performed the thermal transport experiments across a closing nanoscale air gap on two substrates (silicon wafer and AlMg-substrate disk). The experimental results show that the disk-to-head back-heating from the hot spot on the substrate can be directly measured in the case of the AlMg disk (∼ 2–10 °C), while the silicon case shows no back-heating due to its high thermal conductivity. It is demonstrated that the experimental setup is useful to thermal transport studies between two macroscopic surfaces and future development of such microelectronic devices.

Conventional hard disk drive technology, perpendicular magnetic recording (PMR), has reached its superparamagnetic limit of ∼ 1 Tb/in^2 (areal density).[1] To satisfy the storage requirements for worldwide explosive data growth, a new technology called heat-assisted magnetic recording (HAMR) has been proposed to realize a higher areal density.[2,3] HAMR technology uses high coercivity magnetic media with the bit size as small as tens of nanometers to achieve stable data storage and high areal density. The HAMR recording head is integrated with a laser diode, a waveguide, and a near-field transducer (NFT) for laser delivery. A laser beam is launched from the recording head (150–250 °C), and it is focused on the recording disk to locally heat the disk to its Curie temperature (400–500 °C) to assist data writing. Therefore, the HAMR head-disk interface is a system that combines nanoscale spacing (< 15 nm), high temperatures, steep thermal gradient (∼ 10 K/nm), and a high-speed sliding condition (5–40 m/s).

However, the introduction of the laser brings reliability issues to the HAMR head-disk interface.[4,5] The laser induces extra thermal protrusion and thermally-induced material transfer in the interface.[6–9] Also, the laser heats the head and the disk to different extents, which produces thermal transport across the head-disk interface. The laser heating may cause overheating issues at the NFT, and thus affects laser energy delivery and causes head failure.[10,11] Therefore, understanding the thermal transport across the head-disk interface is of great importance to the HAMR technology. Particularly, the back-heating from the disk to the head has been of interest. Previous studies on this topic typically used an external laser source and performed experiments under flying condition.[12,13] Here, we used the built-in laser in the head and operated under non-flying condition for simplification.

[a] Email: qlcheng@berkeley.edu

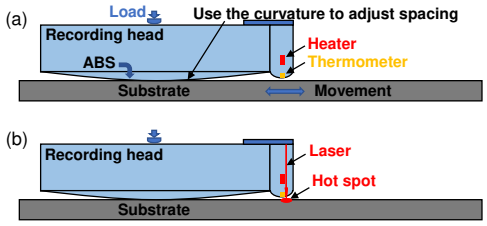

FIG. 1. A schematic diagram of the experimental setup (not to scale). (a) The ABS curvature is used to adjust the initial gap between the thermometer and the substrate. (b) The heater is energized to close the gap with a continuous laser shining on the substrate at the same time.

To study effect of laser on the thermal transport across the HAMR head-disk interface, we built a custom-made non-flying test stage (Figure 1), where the disk is not rotating to exclude the air cooling effect. The experimental setup is also known as static touchdown.[14,15] The air bearing surface (ABS) of the head was loaded onto a substrate, and a nanoscale gap was realized between the two macroscopic surfaces (thermometer and substrate). The initial gap size was adjusted by moving the substrate and using the curvature at the air bearing surface (ABS) of the recording head. For example, when the substrate moves left, the friction between the crowned ABS and the substrate forces the head to tilt and hence the gap size is decreased. Then a heater in the head was energized and a microscale protrusion formed on the head surface due to thermal expansion. Thus, the gap between the head surface and the substrate decreased with the heater power until they were into contact with each other. Meanwhile, a thermometer[16] embedded near the head surface was used to measure its temperature when the head surface approached the substrate. Before con-

tact occurs, the thermal transport between the head protrusion and the substrate is dominated by air conduction and phonon heat conduction, where radiation is negligible.[17] When the gap closes, the heat conduction through the contact (contact heat conduction) dominates. Specifically, Figure 1(b) shows the case with presence of the laser that is integrated within the head, which is analogous to HAMR-type operations. It is noted that this type of HAMR head has a laser spot size ∼ 300 nm and no near-field transducer (NFT). The heater, the thermometer and the laser were controlled by a data acquisition (DAQ) system that consisted of two synchronized Multifunction I/O Devices manufactured by National Instruments: PCI-6115 and USB-6211. They have multiple analog output channels and analog input channels with high sampling rates (∼ MHz). Two substrates were used: a silicon wafer and a commercial multilayered AlMg-substrate PMR disk, considering that they have totally different structures and different thermal properties.

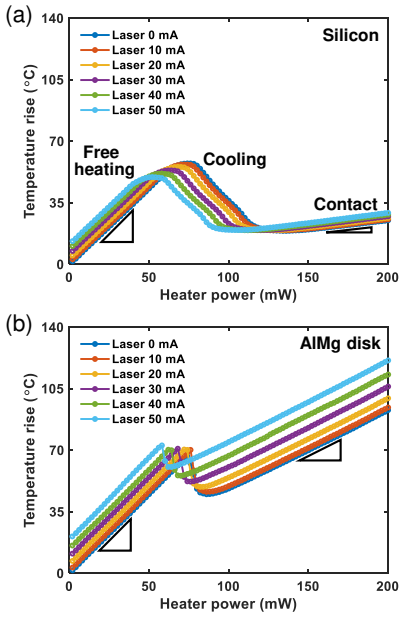

FIG. 2. The temperature rise as a function of the heater power and varying laser currents in two cases of (a) silicon wafer and (b) AlMg disk.

Figure 2 shows the plots of the thermometer temperature rise versus the heater power during static touchdown on the silicon wafer and the AlMg disk, with the laser current varying from 0 to 50 mA. The initial gap size is around 21.3 nm according to the simulation result in Ref[18]. The measured temperatures first increase linearly with the heater power where the air conduction across the gap dominates to almost 2 nm, which is called free heating stage. With the decrease of the gap, enhanced phonon heat conduction dominates and causes a drop in the temperature (cooling stage). Finally, the head protrusion makes contact with the substrate and a much smaller heating slope is observed due to contact heat conduction (contact stage).

Comparing between the two substrates, they show a similar heating slope in the free heating stage (0.87 °C/mW for silicon and 0.91 °C/mW for AlMg disk) because the gap is over several nanometers and air conduction dominates the thermal transport, which is also observed in the silicon/GaAs cases in our previous work.[18] In the contact stage, the silicon wafer case shows a much smaller heating slope (0.11 °C/mW) than that in the AlMg disk case (0.45 °C/mW) because silicon is a better thermal conductor. First, silicon (148 W/(m·K)) has a higher thermal conductivity than AlMg (117 W/(m·K)[19]). Also, the multilayered structure of the disk makes the disk a much poorer thermal conductor. The disk has a lubricant layer (0.1 W/(m·K), ∼ 1 nm thick), carbon overcoat layer (1 W/(m·K), ∼ 2 nm thick) and a magnetic layer (CoCrPt, Ru, CoFe, etc., ∼ 100 nm thick) on the AlMg substrate.[10,20] These layers and the interface thermal conductances between them make the overall effective thermal conductivity of the disk smaller than 117 W/(m·K), leading to the larger heating slope during contact in the static touchdown. During the cooling stage, the AlMg disk presents a smaller temperature drop than the silicon wafer case, which is caused by the total HDI thermal conductance (3×10^7 W/(m^2·K) in the AlMg disk case versus 5×10^7 W/(m^2·K) in the silicon case due to roughness).[17] With a lower HDI thermal conductance, a smaller heater power increase is needed to fill the last ∼ 2 nm of the gap until contact. Thus, the cooling stage in the AlMg disk is short in terms of the heater power. In addition, the AlMg disk case shows a much steeper cooling stage than the silicon case, which

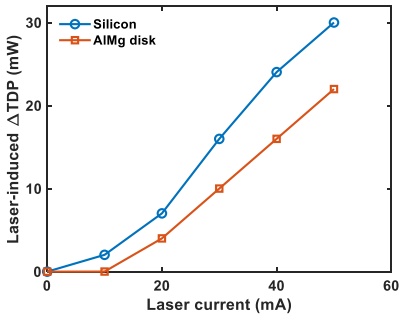

FIG. 3. The laser-induced touchdown power change (ΔTDP).

is likely due to the van der Waals force between the head surface and the disk surface (lubricant layer). The van der Waals force attracts the head protrusion and accelerates the gap's closing, resulting in the faster and steeper cooling stage.

Next, we focus on the laser effect on the experimental results. As the laser current increases, both cases in Figure 2 show that the two critical heater powers, corresponding to the local maximum/minimum of the temperature rise, decrease due to the laser. The reason for this change is that the laser heating causes extra protrusions on the head surface and the disk surface, which reduce the air gap. Hence, smaller heater powers are needed for the two critical points. Additionally, the laser diode in this HAMR head has a threshold $I_{\rm th} \sim 13$ mA, which means that there is no laser coming out in the case of 10 mA laser current. Therefore, the change of the critical heater powers in the case of 10 mA indicates that the laser-induced protrusion does form on the head surface. Figure 3 plots the laser-induced touchdown power change (ΔTDP) in the two cases of silicon wafer and AlMg disk. Here, the touchdown power (TDP) refers to the heater power at the local minimum of the temperature rise, which is exactly between the cooling stage and the contact stage. The ΔTDP represents the gap change due to the laser-induced protrusions. When the laser current is low (< 13 mA), no laser comes out from the head, so there is only an extra laser-induced protrusion on the head surface and the ΔTDP accordingly rises slowly versus the laser current. When the laser current goes beyond 13 mA, another laser-induced protrusion also forms on the silicon surface or disk surface, and as a result, the ΔTDP rises linearly with a larger slope. It is noted that the laser output power has an approximately linear relation with the laser current.[9]

The thermometer temperature rise in Figure 2 is due to both the heater's joule heating and the laser heating. This rise grows linearly with the heater power in the free heating stage and in the contact stage. Thus, the laser heating effect can be obtained by subtracting the laser-off curve from the laser-on curves, which is called laser-induced temperature rise and is plotted in Figure 4(a). Figure 5(a,b) show the schematic diagrams of the head-disk interface in the free heating stage and contact stage. In Figure 4(a), the laser-induced temperature rise is $\sim$ 1–2 °C in the case of 10 mA laser current (below $I_{\rm th}$) due to the laser's joule heat dissipation inside the head, as the laser does not reach the substrate surface. Also, the two stages in the silicon case have smaller laser-induced temperature rises than the AlMg disk case due to the silicon's high thermal conductivity as discussed in Figure 2. When the laser current is over its threshold $I_{\rm th}$, the laser-induced temperature rise is due to two thermal transport mechanisms. One is the laser's joule heat dissipation inside the head as shown in the 10 mA case in Figure 4(a). The other is the heat transfer from the hot substrate surface back to the head, which is known as the disk-to-head back-heating. To isolate the back-heating effect, we assume that the back-heating is negligible in the free heating stage, and that the laser-induced temperature rise due to the laser's joule heat dissipation maintains a constant between the free heating stage and the contact stage with regard to one substrate. The constants can be obtained in the 10 mA case in Figure 4(a) because of lack of the back-heating. Then the laser-induced temperature rise due to the first mechanism can be derived from the value in the free heating stage, and the remaining temperature rise is the back-heating effect, which is plotted in Figure 4(b).

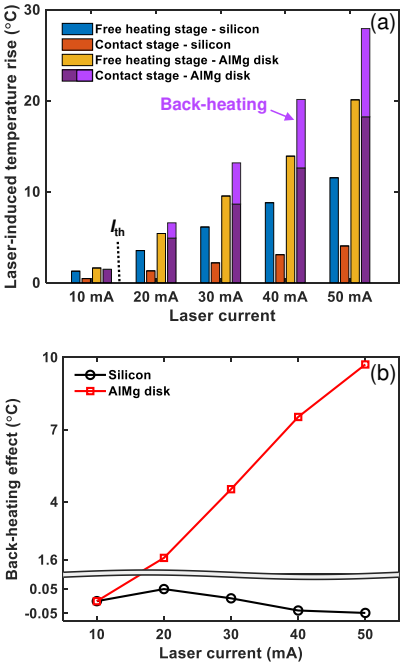

FIG. 4. (a) The laser-induced temperature rise in the free heating/contact stages. The back-heating effect in the AlMg disk case is highlighted as bright purple bars. (b) The back-heating effect in the two cases.

Specifically, in the case of the silicon, the laser heating effect in the contact stage (red bars) is always $\sim$ 65% smaller than that in the free heating stage (blue bars). Figure 4(b) shows that the back-heating effect on silicon is between -0.05 °C and 0.05 °C, which is on the resolution scale, demonstrating that the silicon case shows no back-heating due to its high thermal conductivity. However, the AlMg disk displays a totally opposite result with the presence of the laser. In the cases of 20 mA–50 mA laser currents, the laser heating effect in the contact stage (purple bars) becomes $\sim$ 40% larger than that in the free heating stage (yellow bars), which indicates that

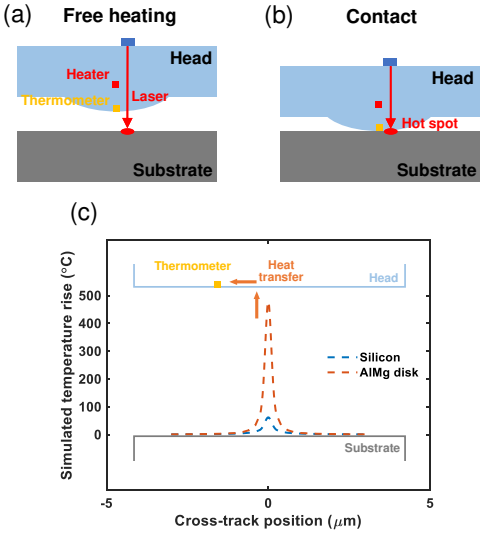

FIG. 5. (a,b) Schematic diagrams of the head-disk interface in the free heating/contact stages. (c) Simulation of the substrate temperature profile showing the back-heating from the hot spot on the substrate to the thermometer.

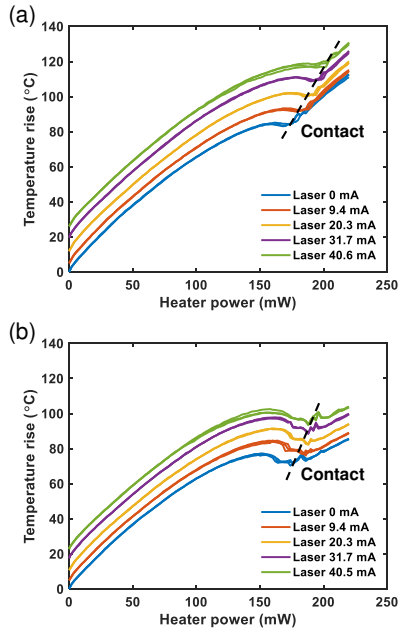

FIG. 6. The temperature rise in the flying cases of a rotating (a) glass-substrate disk and (b) AlMg-substrate disk.

a hot spot forms on the disk due to the laser and in turn heats the head (back-heating) through contact. The bright purple bars in Figure 4(a) highlight the contribution of the back-heating. Figure 4(b) shows that the back-heating effect in the AlMg disk case can be as high as $\sim$ 10 °C and presents a linear relationship with the laser current. The simulation result in Figure 5(c) further validates the discrepancy between the silicon wafer and the AlMg disk, where the silicon and the AlMg disk undergo temperature rises $\sim$ 60 °C and $\sim$ 480 °C respectively under the same laser heating. Under such circumstance, the disk surface is much hotter than the head, and hence transfers heat back to the head through the head-substrate contact, which is sensed by the thermometer. Furthermore, in the case of 10 mA laser current (below I_{th}) without the laser output, Figure 4(a) shows that the laser heating effect in the contact stage (purple bar) is only slightly smaller than that in the free heating stage (yellow bar) because of less contact heat conduction from the disk (compared to silicon) and the absence of back-heating. Therefore, the back-heating effect from the hot spot on the disk can be directly measured on the AlMg disk using the non-flying test stage.

It is noted that the static touchdown experiments differ from the actual HAMR-type operations in that the disk is not rotating and the air cooling is excluded. In the actual HAMR case with the rotating disk as shown in Figure 6, the thermal transport becomes more complicated because the air cooling and frictional heating are involved as compared to the non-flying condition (Figure 2). In Figure 6, the free heating stage shows nonlinearity due to the air cooling as the cooling becomes stronger when the head approaches the rotating disk. After contact occurs, the frictional heating provides extra heating to the thermometer, making the heating slope in the contact stage larger than that in the free heating stage, especially for the glass-substrate disk. Under the flying condition, the heater power change of the critical points ΔTDP as shown in Figure 3 becomes dependent on the ABS design because the introduction of the laser-induced protrusion is likely to change the ABS pressure distribution and the spacing due to its interaction with the surrounding flowing air.

In conclusion, we performed the static touchdown experiments to study the thermal transport across a closing gap between the recording head and the non-rotating substrate. Using the custom-made non-flying test stage, a nanoscale air gap between the head and the substrate can be realized and adjusted. The joule heater in the head was energized to generate a protrusion to reduce the gap until contact occurred. The temperature rise of the thermometer that is positioned near the head surface was measured along with the heater power and the laser current. When the laser comes into play, the laser-

induced protrusions form on the head surface and the disk surface, which contributes to the gap reduction and the ΔTDP. The laser also provides extra heating to the head, and the laser-induced temperature rise is separated from the experimental results. Besides the laser's joule heat dissipation inside the head, a back-heating effect from the hot spot on the disk can be directly measured in the case of the AlMg disk, while the silicon case shows no back-heating due to its high thermal conductivity. This study shows that the non-flying test stage can provide a better understanding of the thermal transport across the HAMR head-disk interface, or generally speaking, between two macroscopic surfaces.

The work was supported by Computer Mechanics Laboratory (CML) at University of California, Berkeley and funded by Advanced Storage Research Consortium (ASRC). We thank Robert Smith, Erhard Schreck, Qing Dai, Sukumar Rajauria and Tan Trinh of Western Digital and Huan Tang of Seagate for supplying the components and providing insightful discussions.

DATA AVAILABILITY

The data and material that support the findings of this study are available from the corresponding author upon reasonable request.

[1]M. Cordle, C. Rea, J. Jury, T. Rausch, C. Hardie, E. Gage, and R. Victora, "Impact of radius and skew angle on areal density in heat assisted magnetic recording hard disk drives," AIP Advances **8**, 056507 (2018).
[2]M. H. Kryder, E. C. Gage, T. W. McDaniel, W. A. Challener, R. E. Rottmayer, G. Ju, Y.-T. Hsia, and M. F. Erden, "Heat assisted magnetic recording," Proceedings of the IEEE **96**, 1810–1835 (2008).
[3]W. Challener, C. Peng, A. Itagi, D. Karns, W. Peng, Y. Peng, X. Yang, X. Zhu, N. Gokemeijer, Y.-T. Hsia, *et al.*, "Heat-assisted magnetic recording by a near-field transducer with efficient optical energy transfer," Nature Photonics **3**, 220–224 (2009).
[4]B. Marchon, X.-C. Guo, B. K. Pathem, F. Rose, Q. Dai, N. Feliss, E. Schreck, J. Reiner, O. Mosendz, K. Takano, *et al.*, "Head–disk interface materials issues in heat-assisted magnetic recording," IEEE Transactions on Magnetics **50**, 137–143 (2014).
[5]J. D. Kiely, P. M. Jones, and J. Hoehn, "Materials challenges for the heat-assisted magnetic recording head–disk interface," MRS Bulletin **43**, 119–124 (2018).
[6]S. Xiong, R. Smith, J. Xu, S. Nishida, M. Furukawa, K. Tasaka, K. Kuroki, Y. Yoon, N. Wang, S. Canchi, *et al.*, "Setting write spacing in heat assisted magnetic recording," IEEE Transactions on Magnetics **54**, 1–7 (2018).
[7]Q. Cheng, H. Wang, S. V. Sakhalkar, and D. B. Bogy, "Measurement of angstrom-level laser induced protrusion using touchdown in heat-assisted magnetic recording," Applied Physics Letters **117**, 153105 (2020).
[8]S. V. Sakhalkar and D. B. Bogy, "Viscoelastic lubricant deformation and disk-to-head transfer during heat-assisted magnetic recording," IEEE Transactions on Magnetics **55**, 1–6 (2018).
[9]Q. Cheng and D. B. Bogy, "Experimental study of smear formation and removal in heat-assisted magnetic recording," Tribology International **165**, 107258 (2022).
[10]J. D. Kiely, P. M. Jones, Y. Yang, J. L. Brand, M. Anaya-Dufresne, P. C. Fletcher, F. Zavaliche, Y. Toivola, J. C. Duda, and M. T. Johnson, "Write-induced head contamination in heat-assisted magnetic recording," IEEE Transactions on Magnetics **53**, 1–7 (2016).
[11]S. Sakhalkar, Q. Cheng, A. Ghafari, and D. Bogy, "Investigation of heat transfer across a nanoscale air gap between a flying head and a rotating disk," Journal of Applied Physics **128**, 084301 (2020).
[12]H. Wu, S. Xiong, S. Canchi, E. Schreck, and D. Bogy, "Nanoscale heat transfer in the head-disk interface for heat assisted magnetic recording," Applied Physics Letters **108**, 093106 (2016).
[13]S. Xiong, R. Smith, E. Schreck, and Q. Dai, "Experimental study of material pick up on heat-assisted magnetic recording (hamr) heads," Tribology Letters **69**, 1–7 (2021).
[14]Y. Ma, A. Ghafari, B. V. Budaev, and D. B. Bogy, "Measurement and simulation of nanoscale gap heat transfer using a read/write head with a contact sensor," IEEE Transactions on Magnetics **53**, 1–5 (2016).
[15]Y. Ma, A. Ghafari, B. Budaev, and D. Bogy, "Controlled heat flux measurement across a closing nanoscale gap and its comparison to theory," Applied Physics Letters **108**, 213105 (2016).
[16]Q. Cheng, S. Rajauria, E. Schreck, R. Smith, N. Wang, J. Reiner, Q. Dai, and D. Bogy, "Precise nanoscale temperature mapping in operational microelectronic devices by use of a phase change material," Scientific reports **10**, 1–8 (2020).
[17]S. Sakhalkar, Q. Cheng, A. Ghafari, Y. Ma, and D. Bogy, "Numerical and experimental investigation of heat transfer across a nanoscale gap between a magnetic recording head and various media," Applied Physics Letters **115**, 223102 (2019).
[18]Q. Cheng, S. Sakhalkar, A. Ghafari, Y. Ma, and D. Bogy, "Dependence of nanoscale heat transfer across a closing gap on the substrate material and ambient humidity," Applied Physics Letters **116**, 213102 (2020).
[19]M. Suk, P. Dennig, and D. Gillis, "Magnetic erasures due to impact induced interfacial heating and magnetostriction," Journal of Tribology **122**, 264–268 (2000).
[20]M. Shamsa, W. Liu, A. Balandin, C. Casiraghi, W. Milne, and A. Ferrari, "Thermal conductivity of diamond-like carbon films," Applied Physics Letters **89**, 161921 (2006).